

Multicellular Rosette Formation Links Planar Cell Polarity to Tissue Morphogenesis

J. Todd Blankenship,¹ Stephanie T. Backovic,¹
Justina S.P. Sanny,¹ Ori Weitz,¹
and Jennifer A. Zallen^{1,*}

¹Developmental Biology Program
Sloan-Kettering Institute
New York, New York 10021

Summary

Elongation of the body axis is accompanied by the assembly of a polarized cytoarchitecture that provides the basis for directional cell behavior. We find that planar polarity in the *Drosophila* embryo is established through a sequential enrichment of actin-myosin cables and adherens junction proteins in complementary surface domains. F-actin accumulation at AP interfaces represents the first break in planar symmetry and occurs independently of proper junctional protein distribution at DV interfaces. Polarized cells engage in a novel program of locally coordinated behavior to generate multicellular rosette structures that form and resolve in a directional fashion. Actin-myosin structures align across multiple cells during rosette formation, and adherens junction proteins assemble in a stepwise fashion during rosette resolution. Patterning genes essential for axis elongation selectively affect the frequency and directionality of rosette formation. We propose that the generation of higher-order rosette structures links local cell interactions to global tissue reorganization during morphogenesis.

Introduction

Convergent extension is a conserved morphogenetic event that generates one of the striking properties of embryonic form—the elongated body axis. A common mechanism for elongation of epithelial and mesenchymal tissues is cell intercalation, in which oriented cell movements cause a tissue to narrow in one dimension and lengthen in a perpendicular dimension (Keller et al., 2000; Wallingford et al., 2002; Nikolaidou and Barrett, 2005; Solnica-Krezel, 2005). Cell intercalation involves a diverse repertoire of behaviors, including polarized protrusive activity (Hardin, 1989; Shih and Keller, 1992; Elul and Keller, 2000; Munro and Odell, 2002), differential adhesion (Wieschaus et al., 1991; Irvine and Wieschaus, 1994), and cell-shape changes (Fristrom, 1988; Bertet et al., 2004). These behaviors are associated with the formation of a polarized cytoarchitecture that concentrates the Bazooka/PAR-3 scaffolding protein and the Myosin II actin motor in distinct cortical domains in *Drosophila* (Bertet et al., 2004; Zallen and Wieschaus, 2004), as well as Par-6 and atypical protein kinase C at sites of motile activity in vertebrates (Hyodo-Miura et al., 2006). However, it is not known

how these polarized proteins engage the cellular machinery that provides the basis for directional cell movement.

In an emerging theme from studies in vertebrates and invertebrates, the spatial information that guides cell intercalation is provided locally by contact between different cell types (Irvine and Wieschaus, 1994; Ninomiya et al., 2004). In *Drosophila*, the *eve* and *runt* transcriptional regulators are expressed in stripes along the developing anterior-posterior (AP) axis, and axis elongation is disrupted when either gene is absent or expressed uniformly (Irvine and Wieschaus, 1994; Zallen and Wieschaus, 2004). Moreover, ectopic *eve* or *runt* expression is sufficient to reorient the polarity of adjacent cells (Zallen and Wieschaus, 2004), demonstrating that polarity is actively modulated by local interactions. A related mechanism operates in vertebrates, where AP differences promote intercalary behavior when *Xenopus* mesodermal cells from different axial positions are juxtaposed in culture (Ninomiya et al., 2004). These studies indicate a deep homology in the spatial mechanisms that organize cell rearrangement during tissue morphogenesis.

Diverse cellular mechanisms translate global spatial cues into directional cell behavior in different tissues. In vertebrates, intercalating cells characteristically elongate in the direction of cell movement (Concha and Adams, 1998; Keller et al., 2000; Topczewski et al., 2001), while no significant cell-shape anisotropy is observed in *Drosophila* (Irvine and Wieschaus, 1994). Here, we show through live imaging studies that intercalating cells in the *Drosophila* germband locally organize to generate multicellular rosette structures that form and resolve in a directional fashion. Germband cells become polarized prior to intercalation through a sequence of events that leads to the asymmetric distribution of F-actin and adherens junction proteins. These polarities are dynamically remodeled during the processes of rosette formation and resolution. Rosette frequency is reduced in *eve* mutants that partially elongate the body axis, and rosette frequency and directionality are both disrupted in *bicoid nanos torso-like* mutants that lack AP patterning and fail to elongate. These results suggest that multicellular rosette structures, and not individual cells or cell interfaces, represent the functional units of cell behavior during tissue elongation.

Results

Planar Polarity Is Established Prior to Intercalation

During axis elongation in *Drosophila*, polarized cell movements cause the embryonic germband to narrow along the dorsal-ventral (DV) axis and lengthen by 2.5-fold along the anterior-posterior (AP) axis (Hartenstein and Campos-Ortega, 1985; Irvine and Wieschaus, 1994). These directional behaviors require the Bazooka/PAR-3 scaffolding protein and the Myosin II actin motor protein, which localize to complementary surface domains along the planar axis (Bertet et al., 2004; Zallen and Wieschaus, 2004). To ask when planar polarity is first

*Correspondence: zallenj@mskcc.org

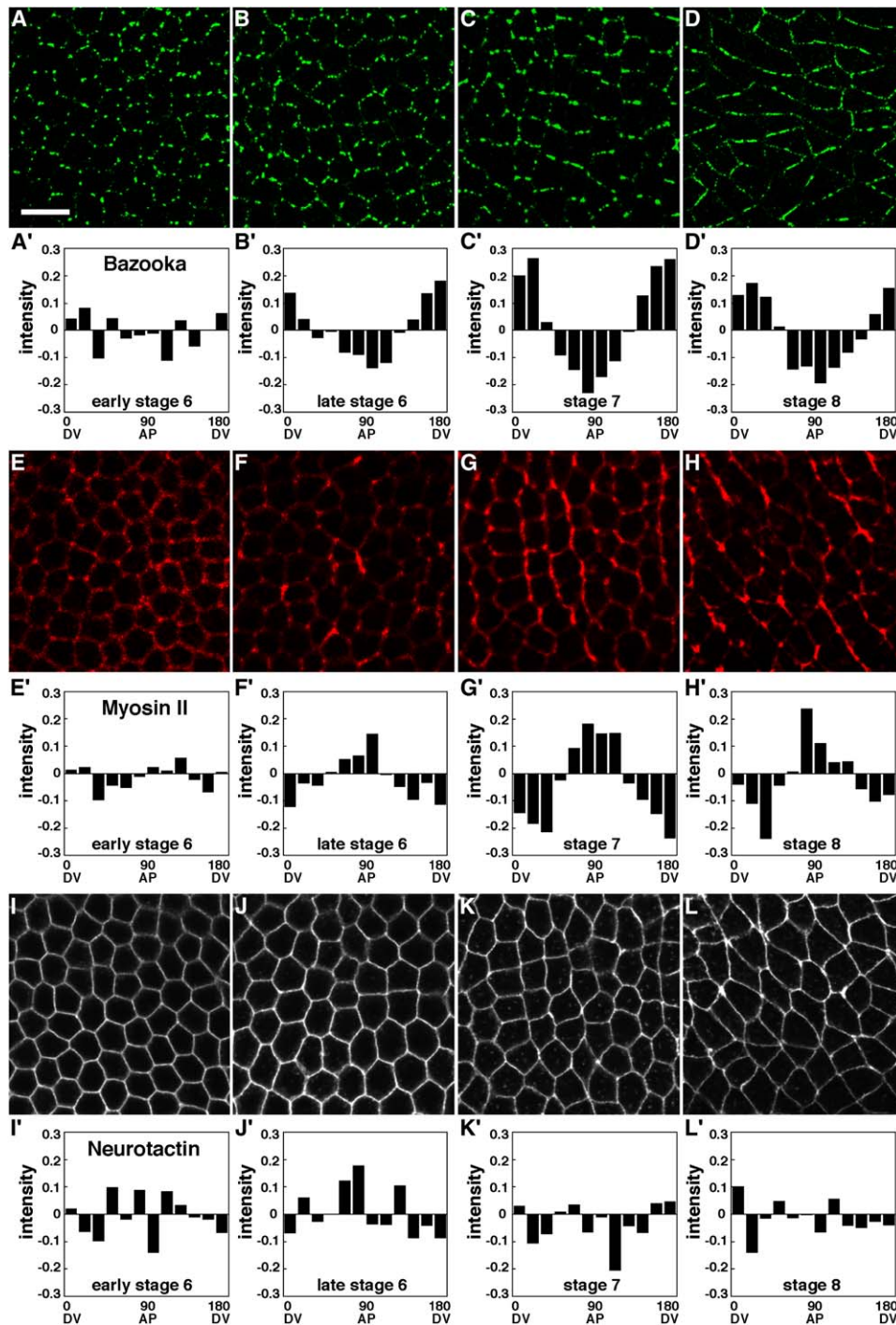


Figure 1. Polarized Localization of Bazooka/PAR-3 and Myosin II Prior to Intercalation

(A–L') (A–D) Bazooka (Baz), (E–H) Myosin II (Myo), (I–L) Neurotactin (Nrt). Anterior is oriented toward the left, and dorsal is up. (A–H) Baz (A) and Myo (E) localized uniformly at the apical surface in early stage-6 embryos. Late stage-6 embryos displayed an enrichment of Baz (B) at horizontal DV interfaces and Myo (F) at vertical AP interfaces. Baz and Myo polarities were also present in stage 7 (C and G) and stage 8 (D and H). (I–L) Nrt was not polarized in (I) early stage 6, (J) late stage 6, (K) stage 7, or (L) stage 8. (A'–L') Relative edge intensities plotted over the full angular range (2–7 embryos/histogram). The same embryos were analyzed for all three proteins. Bars represent the average relative intensity of edges within a 15° angular range. Far-left (0°–14°) and far-right (165°–179°) bars are nearly parallel to the AP axis (DV interfaces); central bars (75°–89° and 90°–104°) are nearly normal to the AP axis (AP interfaces). The scale bar is 10 μm.

generated, we developed a quantitative immunofluorescence assay for protein localization (**Experimental Procedures**). In early stage-6 embryos, Bazooka and Myosin II were localized uniformly at the apical sur-

face (**Figures 1A** and **1E**). By contrast, late stage-6 embryos displayed an enrichment of Bazooka at the borders between dorsal and ventral cells (DV interfaces, **Figure 1B**) and Myosin II at the borders between anterior

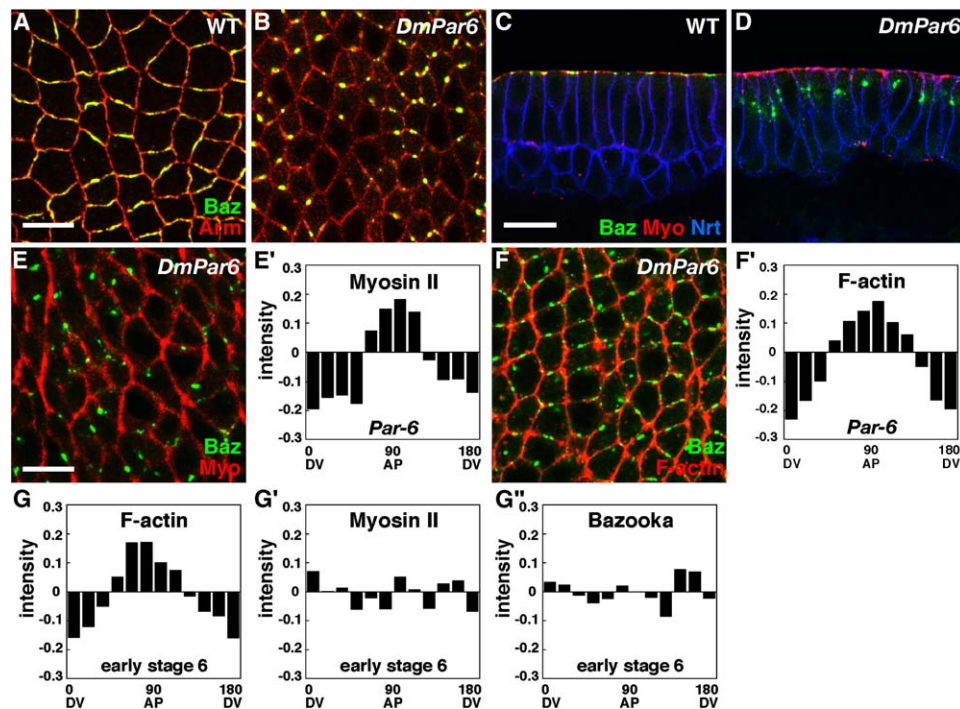


Figure 2. AP Polarity Occurs Upstream or Independently of DV Polarity

(A–G'') (A–F) Bazooka (Baz, green), (A and B) Armadillo (Arm, red), (C–E) Myosin II (Myo, red), (C and D) Neurotactin (Nrt, blue), (F) F-actin (red). Anterior is oriented toward the left, and dorsal is up in (A), (B), (E), and (F); apical is up, and basal is down in (C) and (D). (A,B) Arm (red) and Baz (green) were apical in wild type (A stage 7) and basolateral in *DmPar-6* (B stage 7, shown 6 μm basal to the plane in [A]). Mislocalized Baz puncta retained an affinity for DV interfaces. (C,D) Myo (red) and Baz (green) were apical in wild type (C stage 8), but Baz was basolaterally displaced in *DmPar-6* (D stage 8). (E) Myo polarity (red) was maintained despite Baz mislocalization (green) in *DmPar-6* (stage 8 in [E], stages 7–8 in [E']). (F) F-actin polarity (red) was maintained despite Baz mislocalization (green) in *DmPar-6* (stage 7 in [F], stages 7–8 in [F']). (G) F-actin was polarized in early stage-6 embryos in which Myosin (G') and Bazooka (G'') were uniform (Myosin localization assessed by the functional Sqh:GFP regulatory light-chain fusion). (E', F', and G–G'') Relative edge intensities plotted over the full angular range (2–4 embryos/histogram). Scale bars are 10 μm.

and posterior cells (AP interfaces, Figure 1F). These results indicate that Bazooka and Myosin II initially colocalize at the apical surface and segregate into complementary subdomains during stage 6, prior to the initiation of cell movement. Bazooka and Myosin II remained polarized at the onset of intercalation in stage 7 (Figures 1C and 1G) and throughout intercalation in stage 8 (Figures 1D and 1H). By contrast, the lateral membrane protein Neurotactin was uniformly localized at these stages (Figures 1I–1L; Figure S1, see the Supplemental Data available with this article online). The establishment of a planar polarized cytoarchitecture prior to cell movement is consistent with a role for Bazooka and Myosin II in promoting intercalary behavior.

To ask if AP and DV domains form independently or sequentially, we examined whether Bazooka localization is required for the distribution of other polarized proteins. The *DmPar-6* PDZ-domain protein and *DaPKC* associate biochemically with Bazooka (Wodarz et al., 2000; Petronczki and Knoblich, 2001; Hutterer et al., 2004) and are required for its apical localization (Hutterer et al., 2004; Harris and Peifer, 2005). Bazooka and adherens junction proteins failed to localize apically in *DmPar-6* and *DaPKC* maternal and zygotic mutants, and Bazooka was present in ectopic basolateral puncta that retained an affinity for DV interfaces (Figures 2B and 2D and data not shown). Consistent with these results, germband extension was disrupted in embryos mutant

for *DmPar-6* (49% of progeny of females bearing *DmPar-6* germline clones, $n = 137$) and *DaPKC* (46% of progeny of females bearing *DaPKC* germline clones crossed to *DaPKC* heterozygous males, $n = 167$). Despite the mislocalization of Bazooka and junctional proteins in *DmPar-6* and *DaPKC* mutants, Myosin II localized correctly to AP borders at the apical cell surface (Figures 2D and 2E). These results demonstrate that distinct planar domains of Bazooka and Myosin II can form independently of apical-basal polarity and apical adherens junctions.

F-Actin Polarity Represents the First Break in Planar Symmetry

The asymmetric distribution of Myosin II suggests a structural or functional polarization of the actin cytoskeleton in intercalating cells. Consistent with this possibility, we found that filamentous actin (F-actin) accumulated at AP cell borders in a polarized fashion (Figures 2G and 3A–3C). F-actin was enriched at AP interfaces in early stage-6 embryos in which Bazooka and Myosin II were uniformly distributed (Figure 2G), indicating that Myosin II assembles onto an already polarized F-actin network. Moreover, F-actin polarity was correctly established despite Bazooka mislocalization in *DmPar-6* and *DaPKC* mutants (Figure 2F and data not shown), indicating that AP polarity forms upstream or independently of DV polarity. By contrast, F-actin polarity was abolished

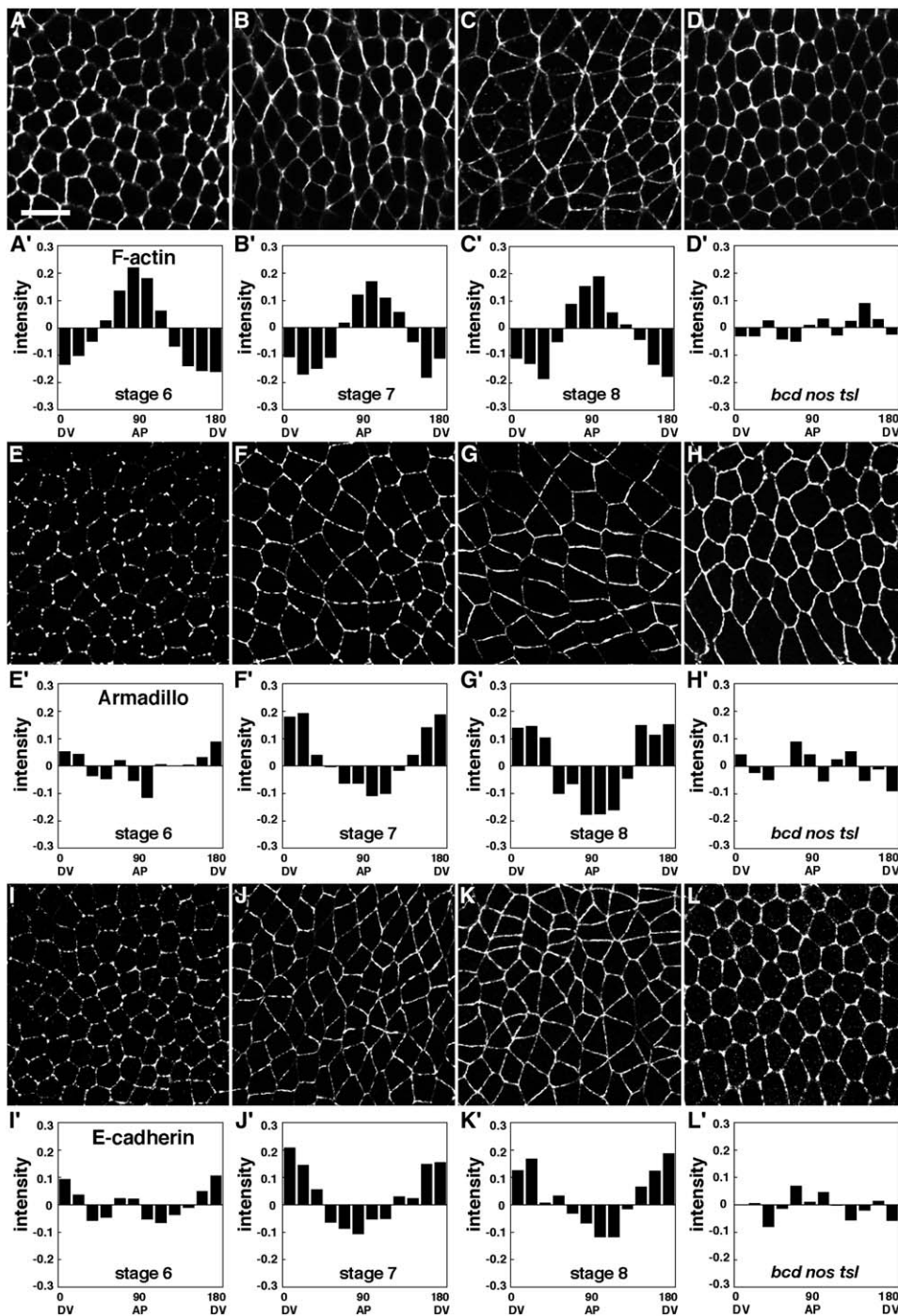


Figure 3. Polarized Localization of F-Actin and Adherens Junction Proteins in Intercalating Cells

(A–L') (A–D) F-actin (visualized with phalloidin), (E–H) Armadillo (Arm), (I–L) DE-cadherin (Ecad). Anterior is oriented toward the left, and dorsal is up. (A–D) F-actin accumulated at AP interfaces in wild-type embryos prior to intercalation in stage 6 (A), at the onset of intercalation in stage 7 (B), and during intercalation in stage 8 (C). F-actin polarity was abolished in *bcd nos tsl* mutants (stage 6 in [D] and [D']). (E–L) Wild-type embryos displayed uniform localization of Arm (E) and Ecad (I) prior to intercalation at stage 6. DV enrichment of Arm (F and G) and Ecad (J and K) was observed at the onset of intercalation in stage 7 (F and J) and during intercalation in stage 8 (G and K). Arm (H) and Ecad (L) were uniformly localized in *bcd nos tsl* mutants (stage 7 in [H] and [L], stages 7 and 8 in [H'] and [L']). (A'–L') Relative edge intensities plotted over the full angular range (3–6 embryos/histogram). The scale bar is 10 μ m.

in the absence of AP patterning in the progeny of *bicoid nanos torso-like* females (*bcd nos tsl* mutants, Figure 3D). Therefore, asymmetric F-actin distribution in response to the AP-patterning system is the first evidence of planar polarity in the *Drosophila* embryo.

Junctional Proteins Are Enriched at DV Interfaces at the Onset of Intercalation

Bazooka and Myosin II accumulate in the vicinity of adherens junctions in intercalating cells (Zallen and Wieschaus, 2004). To ask if adhesion is spatially regulated

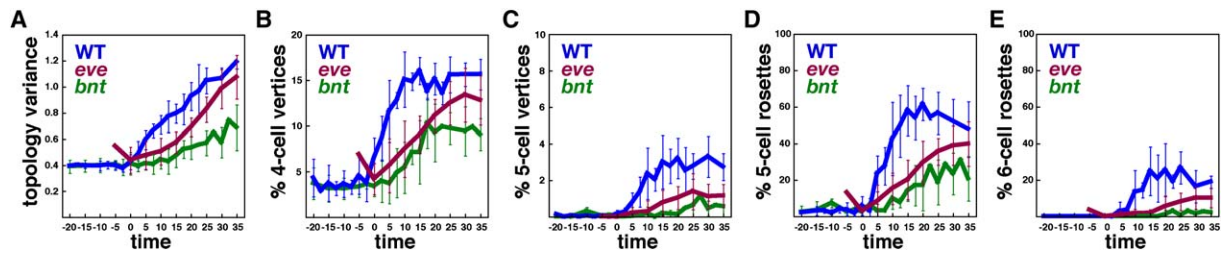


Figure 4. Dynamic Cell Patterns in Intercalating Populations

Wild type (nine embryos, blue), *eve* mutant (seven embryos, red), and *bcd nos tsl (bnt)* mutant (five embryos, green). Bars indicate the mean, and error bars indicate standard error of the mean.

(A) In wild type, the variance of the cell topology (number of sides) distribution, $\sum p(n)(n - \bar{n})^2$, displays a sharp increase in slope at the beginning of stage 7 that provides an objective reference for the onset of intercalation and defines $t = 0$. The variance continued to rise throughout intercalation during stage 7 (0–10 min) and stage 8 (10–35 min). The increase in the topological variance was reduced in *eve* and *bcd nos tsl* mutants.

(B) The fraction of 4-cell vertices increased at the onset of intercalation in stage 7 and plateaued in stage 8 in wild type; *eve* and *bcd nos tsl* mutants displayed a slower rise in 4-cell vertices, and *bcd nos tsl* mutants reached a lower peak value.

(C) Vertices at which five or more cells meet were present in wild-type embryos and were reduced in *eve* and *bcd nos tsl* mutants.

(D) A majority of wild-type cells formed rosettes of five or more cells. Fewer cells formed rosettes in *eve* and *bcd nos tsl* mutants.

(E) Rosettes of six or more cells were present in up to 27% of wild-type cells at a single time point and were less frequent in *eve* and *bcd nos tsl* mutants. Cell patterns in a field of 111–424 cells were analyzed at 2.5 or 5 min intervals.

during intercalation, we examined the distribution of the core adherens junction proteins DE-cadherin/Shotgun and its cytoplasmic binding partner, Armadillo/ β -catenin. While adherens junctions are present at intercellular contacts throughout the germband (Tepass and Hartenstein, 1994), we found that junctional proteins displayed a subtle and reproducible enrichment at DV borders of intercalating cells in stages 7 and 8 (Figures 3F, 3G, 3J, and 3K), but not prior to intercalation at stage 6 (Figures 3E and 3I). The polarized distribution of these junctional proteins was eliminated in *bcd nos tsl* mutants (Figures 3H and 3L). Together, these experiments indicate that F-actin asymmetry is the primary planar polarity in the *Drosophila* germband, followed by the segregation of Myosin II and Bazooka into complementary surface domains. Junctional proteins subsequently become enriched at DV interfaces at the time of intercalation. The asymmetric distribution of cytoskeletal and junctional proteins could contribute directly to polarized cell behavior during tissue elongation.

Cellular Mechanisms of Axis Elongation: Formation of Multicellular Rosette Structures

To understand how this polarized cytoarchitecture is translated into directional cell behavior, we performed time-lapse confocal imaging of embryos expressing GFP-tagged membrane markers (Experimental Procedures; Movie S1). Germband extension occurs over a 2 hr period (Campos-Ortega and Hartenstein, 1985). We focused on the first 40 min, during which 80% of elongation occurs in the absence of cell division (Hartenstein and Campos-Ortega, 1985). Germband cells deviate from a uniform hexagonal organization and display a wide range of neighbor relationships (Zallen and Zallen, 2004). This property is also observed in other epithelial tissues (Fristrom, 1988; Classen et al., 2005). Prior to intercalation, many germband cells were hexagonal in topology, having interfaces with six neighboring cells (58% of cells in 4 stage-6 embryos, >250 cells/embryo). However, a substantial fraction was pentagonal (31%) or heptagonal (9%). The topological range increased at the onset of intercalation in stage 7, and nonhexagonal

cells dominated by stage 8 (73% of cells in 6 stage-8 embryos, >200 cells/embryo). Germband cells therefore become highly disordered during intercalation (Figure 4A) (Zallen and Zallen, 2004).

In a honeycomb, as well as in disordered foams, three cells meet at every vertex (Weaire and Rivier, 1984). Cells that change neighbors in a two-dimensional sheet undergo an obligatory intermediate in which four cells meet; this neighbor-exchange event is referred to as an elementary T1 process (Weaire and Rivier, 1984). Accordingly, the number of 4-cell vertices (vertices at which four cells and four edges meet) increases during intercalation (Figure 4B) (Bertet et al., 2004; Zallen and Zallen, 2004). Our live imaging studies revealed that germband populations form unexpected vertices at which 5 or more cells meet (Figure 4C; Movie S1), with up to 11 cells converging at a single point (Figures 5G–5J). These distinctive multicellular “rosettes” cannot occur through T1 processes and indicate a higher-level organization of cell behavior.

To investigate the behaviors that lead to rosette formation, we developed a computational approach to identify rosette configurations in germband populations (Experimental Procedures). This algorithm highlights clusters of five or more cells that circumscribe short edges (less than one-half the median length) and/or high-order vertices (at which four or more cells meet). In wild-type embryos, up to 61% of germband cells formed rosettes of five or more cells at a single time point (Figure 4D), and up to 27% formed rosettes of six or more cells (Figures 4E and 5A–5F). Similar morphologies were observed in fixed embryos (Figure S2). To detect cells that participate transiently in rosette structures, we tracked individual cells for 20–25 min from the onset of intercalation and found that 87% of germband cells were incorporated into rosettes ($n = 514$ cells in 3 embryos) and that 56% of cells engaged in multiple rounds of rosette formation (up to 5 rosettes/cell that can overlap in time and space, $n = 100$ cells in 3 embryos, average 1.7 rosettes/cell). These results demonstrate that multicellular rosette formation is a prevalent behavior in intercalating populations.

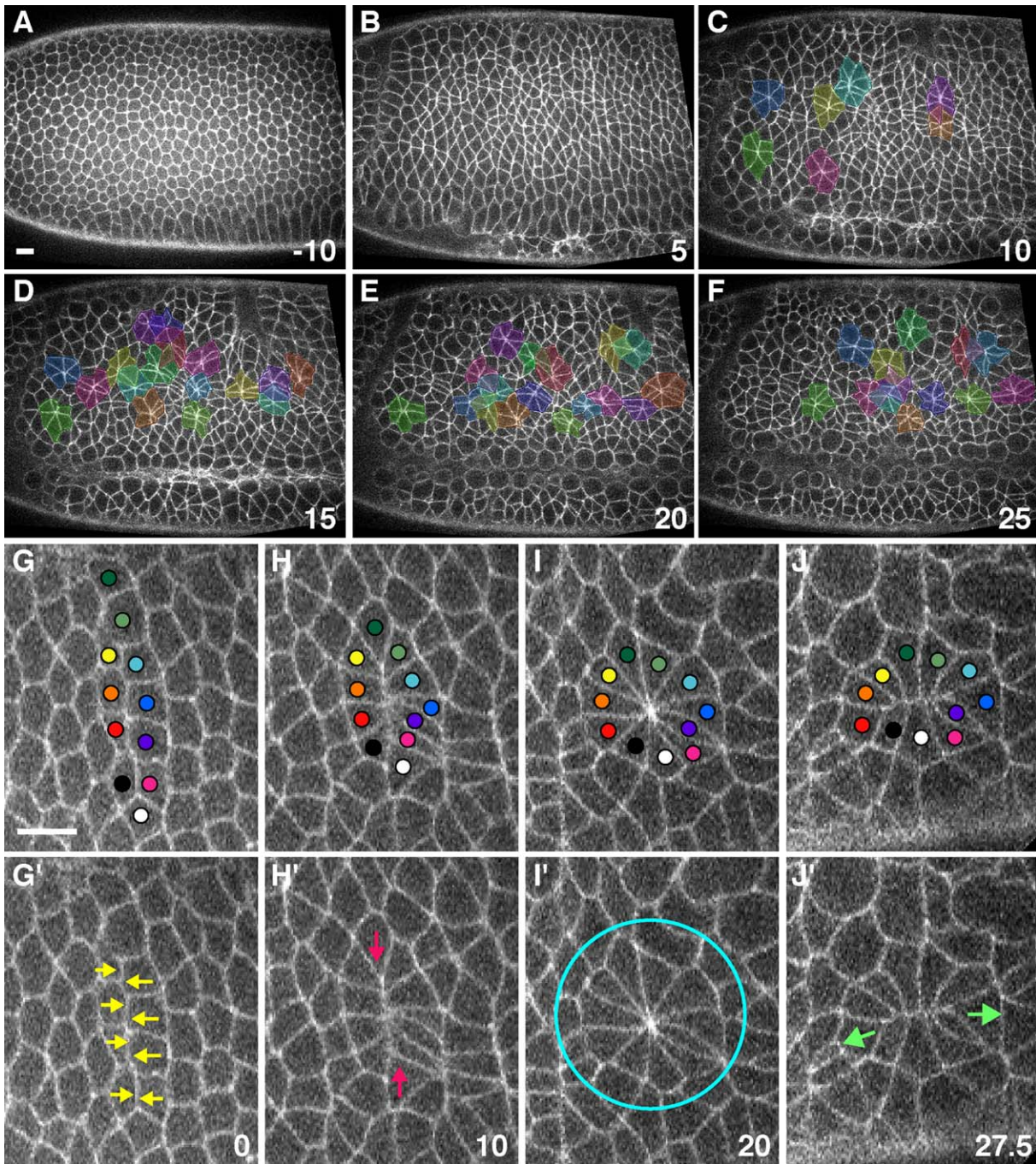


Figure 5. Multicellular Rosette Formation in Intercalating Cells

(A–J) (A–J) Images from a time-lapse movie of wild-type cells expressing GFP:Resille. Time is given in minutes relative to the onset of intercalation as defined in Figure 4A. Anterior is oriented toward the left, and dorsal is up. (A–F) Time-lapse images of the germband delimited by the cephalic furrow (left groove in [B]–[F]) and the ventral furrow (bottom groove in [B]–[F]). Rosettes of six or more cells are highlighted. Colors do not necessarily indicate the same cells in sequential images. (G–J) Time-lapse images of a single rosette. (G) During rosette formation, two columns of cells initially align (edges that will contract are indicated by yellow arrows in [G']). (H) Adjacent pairs of cells constrict their shared interfaces in concert during rosette formation (the direction of convergence is indicated by red arrows in [H']). (I) Multiple cells come into simultaneous contact at a high-order vertex (the 11-cell rosette is indicated by a blue circle in [I']). (J) This apparently symmetric structure resolves in a strictly directional fashion during rosette resolution (the direction of extension is indicated by green arrows in [J']). Scale bars are 10 μm .

Rosette formation and resolution proceed in a strictly directional fashion that parallels structural changes at the tissue level. In every case, a cellular array that was elongated along the DV axis rearranged to form an array that was elongated along the AP axis (100%, $n = 90$

rosettes). Rosette progression consists of three characteristic phases: (1) formation, the constriction of linked interfaces between adjacent columns of cells (Figure 5H, ~10 min); (2) a transient high-order vertex intermediate in which multiple cells meet at a single point

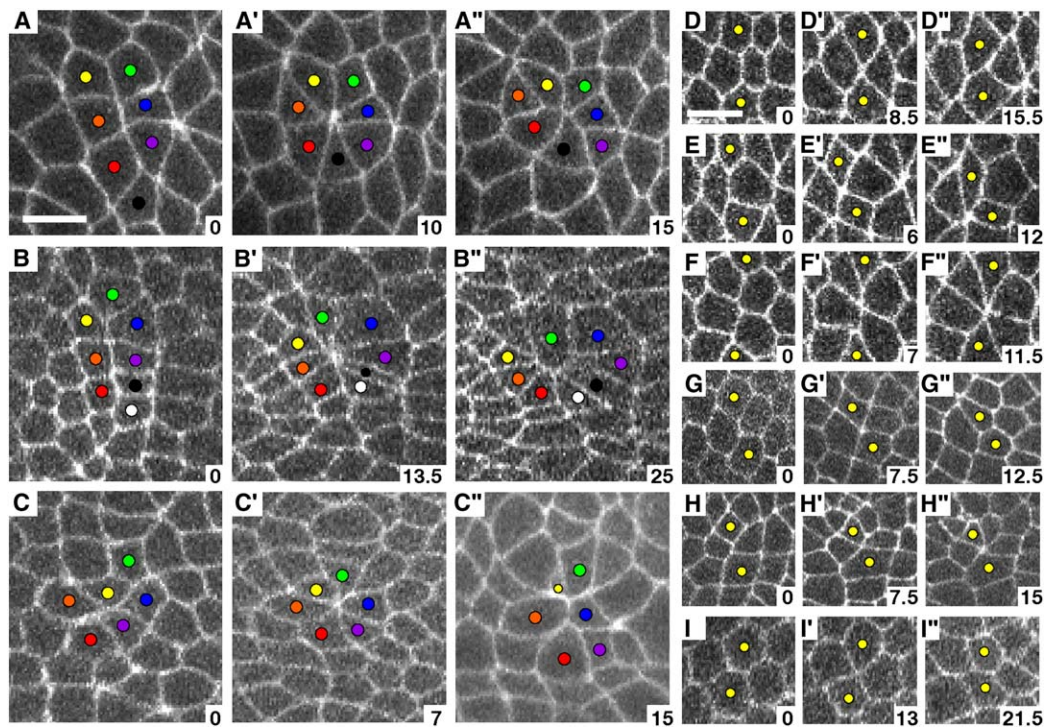


Figure 6. Rosette Behaviors Are Directional in *eve*, but Not *bcd nos ts1* Mutants

(A–I′) Images from time-lapse movies of intercalating cells in wild type (A and D–F), *eve* mutants (B, G, and H), and *bcd nos ts1* mutants (C and I) visualized with GFP:Resille (A, C–F, and I) or GFP:Spider (B, G, and H). Time is given in minutes. Anterior is oriented toward the left, and dorsal is up. (A) Wild-type rosette progression causes a multicellular array to narrow along the DV axis during rosette formation (A′) and to elongate along the AP axis during rosette resolution (A′′). (B) In an *eve* mutant, 6-cell rosettes formed (B′) and resolved (B′′) in a directional fashion. (C) In a *bcd nos ts1* mutant, 6-cell rosettes formed (C′) and resolved (C′′) along random axes. (D–F) Wild-type 4-cell vertices (D′–F′) formed through loss of an AP interface and resolved to create contact between dorsal and ventral cells (D′′ and E′′) or to join rosettes (F′′). (G and H) In *eve* mutants, 4-cell vertices resolved (G′′) or joined rosettes (H′′) with wild-type directionality. (I) In *bcd nos ts1* mutants, 4-cell vertices often formed through loss of a DV interface (I′), and new edges often restored old contacts (I′′). Scale bars are 10 μ m.

(Figure 5I, <1 min); and (3) resolution, the establishment of contact between cells that were previously 2–5 cell diameters apart along the DV axis and the separation of cells that had been immediate AP neighbors (Figure 5J, ~10 min). Rosette behaviors produced a change in the AP/DV aspect ratio (the length of a multi-cell array along the AP axis divided by its length along the DV axis) by a factor of 2.1 for rosettes of 6–7 cells ($n = 74$) and by a factor of 3.0 for rosettes of 8–10 cells ($n = 9$). The change in the aspect ratio for the germband sheet during the same time period was 2.7 ± 0.2 (for a field encompassing one-third of the germband, $n = 3$ embryos).

The directionality of rosette formation arises from the concerted contraction of AP interfaces shared by neighboring pairs of cells. Five-cell rosettes formed by loss of two linked AP interfaces (98%, $n = 190$), 6-cell rosettes formed by loss of 3 linked AP interfaces (100%, $n = 65$, Figures 6A and 6F), and up to 8 linked AP interfaces contracted in tandem to produce rosettes of 7–11 cells (100%, $n = 25$, Figures 5G–5I). Contraction of isolated AP interfaces leads to local interactions among four cells that can also result in neighbor exchange (T1 processes [Weaire and Rivier, 1984]) and have been implicated in germband elongation (Bertet et al., 2004). Consistent with this, 99% of 4-cell vertices formed through loss of an AP interface ($n = 376$, Figures 6D–6F), and 72% of 4-cell vertices resolved by T1 processes ($n = 715$, Figures 6D and 6E). These events created con-

tact between cells that were separated by less than one cell diameter along the DV axis (92%, $n = 391$) and increased the AP/DV aspect ratio by a factor of 1.79 ($n = 17$). T1 neighbor exchange as previously described (Bertet et al., 2004) therefore contributes to axis elongation and represents one manifestation of the general cell behaviors that can also lead to rosette formation. However, the dynamic behaviors of linked interfaces in forming rosette structures were distinct from isolated interfaces. AP interfaces rapidly contracted to form 4-cell vertices during T1 neighbor exchange (average time to disappearance 7.5 ± 0.3 min, $n = 56$ interfaces in 3 embryos). By contrast, AP interfaces in forming rosettes persisted significantly longer before collapsing to produce a high-order vertex (10.8 ± 0.5 min, $n = 49$ interfaces in 3 embryos) and were more likely to undergo alternating rounds of contraction and extension (Movie S1). These results suggest that interface dynamics are actively modulated by input from neighboring pairs of cells in a mechanism that promotes rosette formation.

Dynamic Protein Localization during Rosette Formation and Resolution

To understand the molecular basis of rosette behavior, we analyzed the localization of cytoskeletal and junctional proteins in fixed cells that display morphological hallmarks of rosette formation and resolution. F-actin and Myosin II were enriched in high-order vertices at

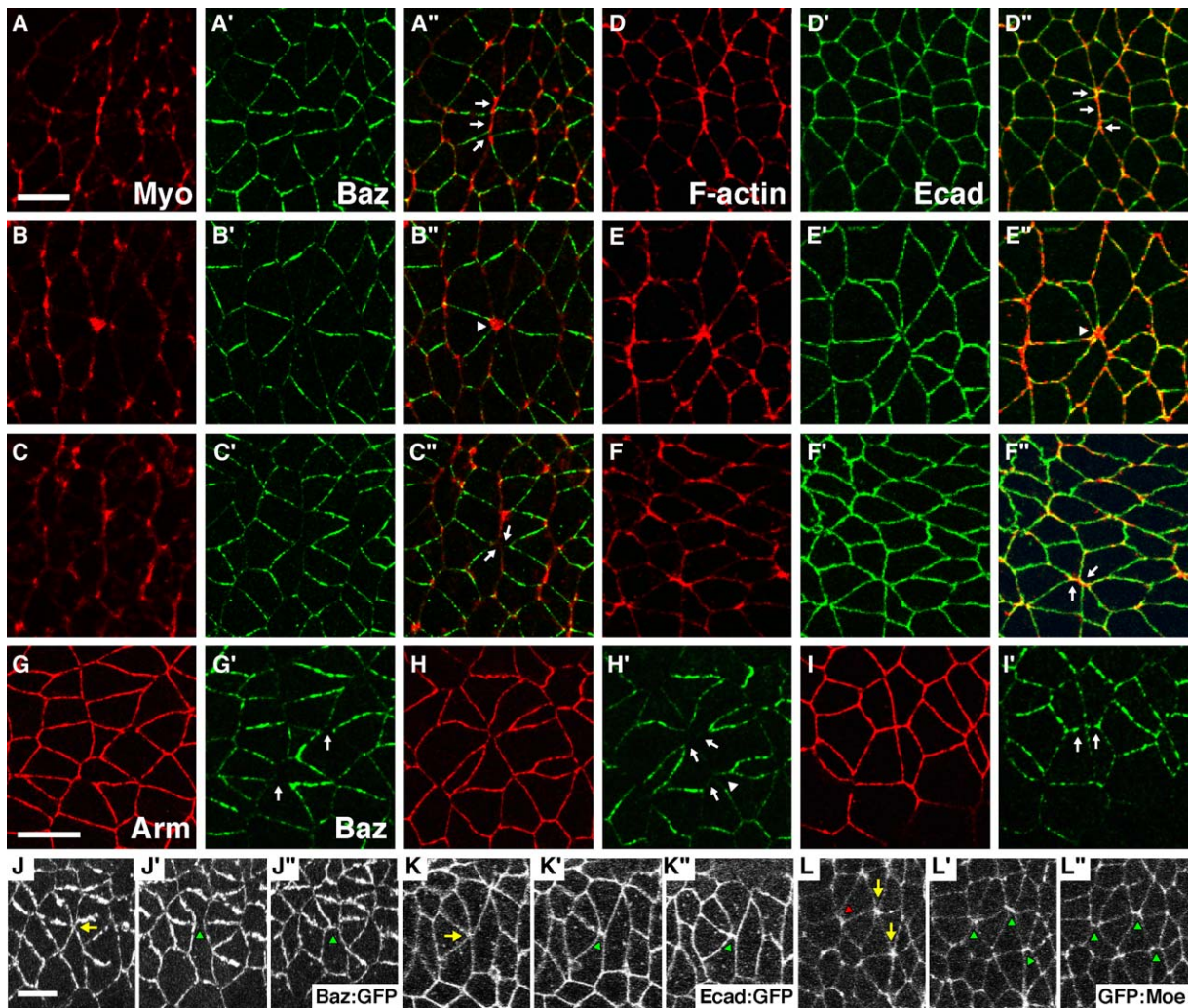


Figure 7. Dynamic Localization of Cytoskeletal and Junctional Proteins during Rosette Progression

(A–L'') (A–C) Myosin II (Myo, red), (A'–C' and G'–I') Bazooka (Baz, green), (D–F) F-actin (red), (D'–F') DE-cadherin (Ecad, green), (G–I) Armadillo (Arm, red). Anterior is oriented toward the left, and dorsal is up. (A–C) Myo was enriched in shrinking AP interfaces in forming rosettes (arrows in [A'']) and at high-order vertices (arrowhead in [B'']). Baz was depleted from growing DV interfaces in resolving rosettes (arrows in [C'']). (D–F) F-actin was enriched in shrinking AP interfaces in forming rosettes (arrows in [D'']), in high-order vertices (arrowhead in [E'']), and in growing DV interfaces in resolving rosettes (arrows in [F'']). (G–I) Short DV interfaces either lacked Arm (G) and Baz (G' arrows point to missing edges, 4/25 rosettes), displayed high levels of Arm (H) and low levels of Baz (arrows in [H'], 19/25 rosettes), or were positive for Arm (I) and Baz (arrowhead in [H'] and arrows in [I'], 2/25 rosettes). Similarly, a majority of short DV interfaces displayed high levels of Ecad and low levels of Baz (11/15 rosettes), while a subset was negative for both (1/15 rosettes) or positive for both (3/15 rosettes). (J–L) Images from a time-lapse movie of wild-type cells expressing (J) Bazooka:GFP, (K) Ecad:GFP, or (L) GFP:Moesin. Vertices (yellow arrows), growing edges (green arrowheads), and shrinking edges (red arrowheads) are indicated. Bazooka:GFP was recruited to new interfaces after a delay ([J'], $t = 5$ min; [J''], $t = 11$ min), while Ecad:GFP was present at new interfaces from the earliest stages of interface formation ([K'], $t = 0.5$ min; [K''], $t = 2.5$ min). (L) GFP:Moesin accumulated transiently at new interfaces ([L'], $t = 2$ min) and quickly returned to steady-state levels ([L''], $t = 3$ min, GFP remains enriched at the interface indicated by the central arrowhead). Scale bars are 10 μ m.

the rosette center (Figures 7B and 7E) and in linear chains of short AP interfaces in configurations that resemble forming rosettes (compare Figures 7A and 7D with Figures 5H and 6A). Resolving rosettes were identified by linear chains of short DV interfaces and the characteristic hourglass morphology of associated cells (compare Figures 7C and 7F with Figures 5J and 6A''). In contrast to its general association with AP interfaces, F-actin was also enriched at DV interfaces in resolving rosettes (Figure 7F). A majority of these interfaces displayed gaps in Bazooka localization (Figures 7C', 7G', and 7H'; 43/49 rosettes), but they were usually positive

for DE-cadherin (Figure 7F'; 14/15 rosettes) or Armadillo/ β -catenin (Figure 7H; 21/25 rosettes). Apparent gaps between cells stained positively for the Neurotactin membrane marker (data not shown), demonstrating the presence of membranes in these regions. F-actin enrichment and Bazooka depletion at newly forming DV interfaces do not correlate with their global distribution and suggest a role in rosette resolution.

These results are consistent with a model in which DE-cadherin and Armadillo/ β -catenin are recruited to sites of new cell contacts prior to Bazooka association. To test this directly, we analyzed protein localization in

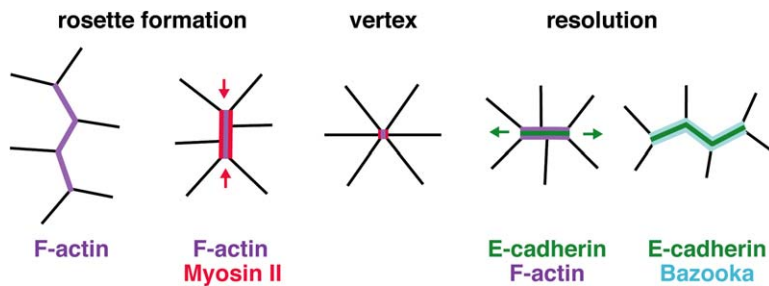


Figure 8. Multicellular Rosette Formation and Axis Elongation

Sequence of events from left to right. F-actin enrichment (purple) at AP interfaces is the earliest evidence of planar polarity (left). Myosin II (pink) subsequently accumulates at AP interfaces and may coordinate the contraction of linked edges to drive rosette formation. F-actin and Myosin II colocalize at the vertex where multiple cells meet (center). Rosettes resolve in a directional fashion to create contact between cells that were previously separated along the DV axis.

DE-cadherin association (green) is an early step in new contact formation and coincides with formation of a transient F-actin structure (right). Bazooka (blue) is recruited to new interfaces after a delay, which may create local differences in adhesion that are important for rosette resolution.

living embryos that express functional GFP fusions to DE-cadherin (Oda and Tsukita, 2001) or Bazooka (Benton and St. Johnston, 2003). We found that DE-cadherin:GFP accumulated at new interfaces from the earliest time points examined, within 30 s of the appearance of a detectable edge between cells (0.6 ± 0.1 min, $n = 10$ rosettes; Figure 7K). By contrast, Bazooka:GFP was first detected at new interfaces after a delay of several minutes (3.8 ± 0.6 min, $n = 10$ rosettes; Figure 7J). The F-actin marker GFP:Moesin (Kiehart et al., 2000) was enriched at new interfaces within 30 s of their formation and then returned to steady-state levels (within 2.3 ± 0.2 min, $n = 13$ rosettes; Figure 7L). These results demonstrate that cell contacts created by intercalation first accumulate DE-cadherin and F-actin and subsequently recruit Bazooka during their eventual stabilization (Figure 8).

Rosette Frequency and Directionality Require AP Patterning

We have shown that a majority of germband cells participate in multicellular rosette structures that undergo directional convergence and extension. If rosette behaviors are important for elongation, then germband extension should be disrupted in mutants that form fewer rosettes or rosettes that lack directionality. To test these predictions, we performed time-lapse imaging of *eve* mutants that display reduced germband elongation (Irvine and Wieschaus, 1994) and *bcd nos tsl* mutants that fail to elongate (Nusslein-Volhard et al., 1987). These experiments revealed that fewer rosettes formed in *eve* and *bcd nos tsl* mutants (Movies S2 and S3). The peak fraction of cells in rosettes at a single time point decreased from 61% in wild-type embryos to 40% in *eve* and 31% in *bcd nos tsl* (Figure 4D), and rosettes of six or more cells decreased from 27% in wild-type to 10% in *eve* and 3% in *bcd nos tsl* (Figure 4E). Consistent with these results, fewer 4-cell vertices joined rosettes in *eve* (14%, $n = 448$) and *bcd nos tsl* (11%, $n = 265$) compared to wild-type (27%, $n = 715$). In addition, less than 2% of wild-type 4-cell vertices failed to either resolve or join a rosette within 15 min, while 20% of 4-cell vertices in *eve* mutants and 18% of 4-cell vertices in *bcd nos tsl* mutants persisted for 15 min or longer. The failure to form higher-order rosettes in AP-patterning mutants is thus accompanied by an aberrant stabilization of 4-cell intermediates.

Surprisingly, some rosettes still formed despite the absence of AP-patterning information in *bcd nos tsl* mutants, but these behaviors occurred along random axes

and did not promote elongation. In *eve* mutants, 4-cell vertices formed through contraction of an AP interface as in wild-type (93%, $n = 328$, Figures 6G and 6H), while 4-cell vertices in *bcd nos tsl* often formed through loss of a DV interface (64%, $n = 237$, Figure 6I). Similarly, 6-cell rosettes in *eve* mutants formed and resolved with wild-type directionality (12/13, Figure 6B), while 6-cell rosettes in *bcd nos tsl* mutants formed through loss of DV interfaces (6/11), AP interfaces (3/11), or both (2/11, Figure 6C) and resolved to promote elongation (4/9), oppose elongation (4/9), or produce no change in dimension (1/9). A subset of 6-cell rosettes in *bcd nos tsl* mutants formed and resolved along the same axis, restoring an interface that had recently been lost (5/9 rosettes). These results demonstrate that rosette resolution does not always occur perpendicular to the direction of rosette formation and suggest that both processes are regulated downstream of the AP-patterning system.

Discussion

A major challenge in developmental biology is to understand how changes in tissue structure are generated on a cellular and molecular level. Here, we demonstrate that cytoskeletal and junctional proteins in intercalating cells are polarized with respect to the axes of the embryo and are dynamically remodeled during rosette formation and resolution. Three lines of evidence indicate that rosette structures are closely associated with the essential cell behaviors that drive axis elongation. First, rosettes form and resolve in a strictly directional fashion that results in the convergence and extension of a cellular array in accordance with structural changes at the tissue level. Second, a majority of germband cells participate in multicellular rosette structures. Third, rosette frequency and directionality are selectively disrupted in AP-patterning mutants that are defective for axis elongation. Rosette behaviors account for morphological properties of germband populations that cannot be explained by simple neighbor exchange, including the diverse cell geometries present in intercalating populations, the meeting of more than four cells at a single point, and the rapid juxtaposition of widely separated cells.

Creating Asymmetry along Planar Axes

The first evidence of planar polarity in intercalating cells is an asymmetric enrichment of F-actin in response to the AP-patterning system. Cytoskeletal reorganization is also an early event in polarization of the *C. elegans*

embryo in response to sperm entry (Nance, 2005). F-actin polarity in the *Drosophila* germband is followed by segregation of Myosin II and Bazooka into distinct cortical domains and enrichment of adherens junction proteins at DV interfaces. Polarized F-actin and Myosin II distribution does not require proper Bazooka localization to DV interfaces, indicating that AP polarity forms upstream or independently of DV polarity. These results argue that Bazooka does not delimit the boundary of Myosin II expression, since reduction of the Bazooka DV domain in *DmPar-6* and *DaPKC* mutants is not accompanied by an expansion of Myosin II. Moreover, apical Myosin II does not simply exclude Bazooka, since Bazooka aggregates display an affinity for DV interfaces at basolateral locations. These results indicate that planar polarized Bazooka and Myosin II domains can form in the absence of direct contact upon disruption of apical-basal polarity.

Actin-Myosin Cables Align across Multiple Cells during Rosette Formation

It has been proposed that axis elongation in *Drosophila* occurs through stereotyped cell-shape changes across a uniform field (Bertet et al., 2004). However, germband cells display a wide range of geometries, and only a subset of cells is present in the prescribed orientation prior to intercalation (Zallen and Zallen, 2004). Moreover, this model stipulates a single round of intercalation, whereas multiple rounds are required for full elongation. Here, we find that germband cells display a range of dynamic behaviors within a topologically disordered population that allow for both simple neighbor exchange and higher-order rosette formation. Actin-myosin networks could coordinate interface contraction in adjacent pairs of cells to create multicellular rosette structures that amplify the elongation produced by local cell rearrangement. Supracellular actin-myosin cables are implicated in morphogenetic processes such as wound healing (Martin and Lewis, 1992; Wood et al., 2002), epithelial closure (Young et al., 1993; Jacinto et al., 2002; Franke et al., 2005), and cell sorting (Wei et al., 2005). Of note, germband cells in *bcd nos tsl* mutants still undergo rosette formation in the absence of AP patterning, but it is nondirectional. The capacity for locally coordinated cell-shape changes may represent an intrinsic property of epithelial tissues that can be mobilized in response to distinct spatial inputs during morphogenesis.

Dynamic Regulation of Adherens Junction Proteins during Intercalation

Differential adhesion could influence cell behavior at two stages of germband extension: first, through the general enrichment of junctional proteins at DV interfaces, and, later, through transient differences in junctional composition at new cell contacts. The asymmetric distribution of Bazooka prefigures the formation of a planar polarized junctional network, consistent with known roles of Bazooka in promoting the assembly or stabilization of adherens junctions (Muller and Wieschaus, 1996; Abdelilah-Seyfried et al., 2003; Harris and Peifer, 2004; Chen and Macara, 2005). Adhesive differences could perform multiple functions during intercalation, such as facilitating the alignment of cells prior to rosette initiation, providing structural support for the extreme morphologies

produced by rosette formation, or promoting membrane growth during rosette resolution.

We demonstrate that high-order vertices at which five or more cells meet are resolved through a mechanism that involves AP patterning and sequential recruitment of cytoskeletal and junctional proteins at new membranes. Nascent cell contacts display a transient F-actin accumulation and Bazooka depletion that could contribute to dynamic junctional behaviors required for membrane growth. In cultured cells, F-actin promotes the expansion of junctional domains in a polymerization-dependent process mediated by the Arp2/3 complex and formin-1 (Kovacs et al., 2002; Kobiela et al., 2004; Verma et al., 2004). To our knowledge, our data provide the first evidence that F-actin is recruited to newly forming junctions in vivo, where it may influence the formation or stabilization of cell contacts.

While the sequential association of cytoskeletal and junctional proteins may contribute to the formation of new cell interfaces, this does not explain why rosettes resolve in a directional fashion. The simultaneous association of multiple cells provides a potential choice point at which cells select new neighbors in a reproducible manner. It has been proposed that 4-cell vertices allow a cell to choose among three neighbors (Baum, 2004). Here, we find that rosette formation can bring up to 11 cells into simultaneous contact, providing an opportunity for a cell to choose among multiple possible interactions. The guidance information that directs this choice is provided by the AP-patterning system, since rosette resolution in *bcd nos tsl* mutants does not correlate with the axis of rosette formation or the global axes of the embryo. Moreover, 4-cell interactions are aberrantly stabilized in *eve* and *bcd nos tsl* mutants, suggesting that these structures are not intrinsically unstable, but are actively resolved by specific cell affinities. The AP-patterning system may allow a cell to precisely discriminate among its neighbors during rosette resolution. Alternatively, disassembly of the contractile actin-myosin network involved in wild-type rosette formation could render a subset of cells refractory to building the actin structures required to establish new contacts.

Emergent Patterns of Tissue Organization Arise from Single-Cell Behaviors

The study of morphogenesis lies at the interface between cell and tissue biology and requires new ways of thinking about cell behavior. An outstanding question is whether the organization of multicellular populations can be described as the sum of single-cell events, or if unique phenomena emerge at the tissue level. Individual cells often coordinate their behavior within a cohesive multicellular structure. Perhaps the functional unit of tissue morphogenesis is in fact a group of cells, each of which senses its position within the group and carries out distinct behaviors accordingly. For example, the monolithic advance of a cell sheet mediates wound healing and epithelial closure (Schock and Perrimon, 2002; Redd et al., 2004), and entire tissues can migrate as a group to new locations in the body (Lecaudey and Gilmour, 2006). In these cases, it may be appropriate to consider tissue morphogenesis in terms of collective actions by multi-cell assemblies, rather than as the reiteration of single-cell behaviors. We show here that

multicellular rosette structures promote rapid and efficient tissue elongation in the *Drosophila* germband. An understanding of the principles that govern such higher-order cell behaviors will provide insight into how local interactions between cells generate complex properties of tissue organization.

Experimental Procedures

Fly Stocks and Genetics

Flies were maintained at 25°C by standard procedures. Oregon R was the wild-type stock. Germline clones for the *DaPKC*^{K06403} (Wodarz et al., 2000) and *DmPar-6*^{Δ226} (Petronczki and Knoblich, 2001; Hutterer et al., 2004) alleles were generated by the FLP-DFS system (Chou and Perrimon, 1992). Time-lapse imaging was conducted with GFP:Resille (II) and GFP:Spider (III) lines, gifts from Alain Debec. Zygotic *eve* mutant progeny from an *eve*^{R13/CyO}; GFP:Spider stock were imaged starting at stage 6b/7 and were genotyped by cephalic furrow defects and partial germband extension. Maternal *bcd nos tsl* mutant embryos were progeny of GFP:Resille; *bcd*^{E1 nos}^{L7} *tsl*¹⁴⁶ females. Bazooka:GFP embryos were the F2 progeny of UASp:Bazooka:GFP (Benton and St. Johnston, 2003) and *matα:UASp:Gal4VP16* 67C;15 (gift of D. St. Johnston). Ecad:GFP (Oda and Tsukita, 2001), GFP:Moesin (Kiehart et al., 2000), and Sqh:GFP (Royou et al., 2004) were expressed from endogenous promoters.

Immunohistochemistry

Embryos were fixed by heat-methanol fixation (Muller and Wieschaus, 1996) for staining with rabbit anti-Arm (1:200 [Riggleman et al., 1990]), guinea pig anti-Baz (1:500, made by J.A.Z. as described by Wodarz et al., [1999]), rabbit anti-Myo II (Zipper heavy chain, 1:1250, gift of C. Field [Foe et al., 2000]), and mouse anti-Nrt (1:200, Developmental Studies Hybridoma Bank, DSHB). Embryos were fixed for 1 hr at the interface of heptane and 3.7% formaldehyde in 0.1 M sodium phosphate buffer (pH 7.4) and were manually devitellinized for staining with Alexa-488 phalloidin (Molecular Probes), guinea pig anti-Baz (1:500), rat anti-DE-cadherin (1:100 [Oda et al., 1994], DSHB), and rabbit anti-GFP (1:100, Torrey Pines). Secondary antibodies (1:500) were conjugated to Alexa-488, Alexa-568, or Alexa-647 (Molecular Probes). Embryos were mounted in Prolong Gold (Molecular Probes). Images were acquired on a Zeiss LSM510 META confocal microscope with a PlanNeo 40×/1.3NA objective.

Quantitation of Polarized Protein Distribution

Embryos were staged as described by Campos-Ortega and Hartenstein (1985); stage-6 embryos displayed no pole cell movement and do not include embryos in 6a or 6b. Images were maximum-intensity projections of up to eight 1 μm apical slices acquired at 0.5 μm steps to accommodate stage-specific differences in apical-basal distribution. F-actin and Myosin II were analyzed in projections of the same z-slices as DE-cadherin and Bazooka, respectively. Edge orientation and mean fluorescence intensity were measured in Object Image for all edges in a 50 μm² region (73–276 interfaces/embryo). Absolute fluorescence intensities were ranked and normalized to a scale from -0.5 to 0.5 to generate relative intensity values that were negative for edges with below-average intensity and positive for edges with above-average intensity. Distributions were scored as polarized if all positive and negative bars were consecutive.

Time-Lapse Acquisition

In Figures 4 and 5, Z stacks of 1 μm steps were acquired at 15 s intervals on a Perkin Elmer RS5 spinning disc confocal microscope with a Zeiss PlanNeo 40×/1.3NA objective. Single optical slices (GFP:Resille) or projections of 1–3 slices (GFP:Spider) within 3 μm of the apical surface were analyzed. In Figures 7J–7L, Z stacks of 1 μm slices at 0.5 μm steps were acquired at 30 s intervals on a Zeiss LSM510 META confocal microscope with a PlanNeo 40×/1.3NA objective. For Bazooka:GFP and Ecad:GFP, maximum-intensity projections of 7–9 apical slices were generated in Volocity (Improvision), and mean interface intensity was measured in ImageJ. Interfaces were scored as positive if they reached >50% of their final intensity (average of ten steady-state measurements) after subtracting background intensity (average of ten cytoplasmic measurements).

Time-Lapse Analysis

Confocal images were analyzed in a semiautomated fashion by using custom software written in Matlab. A binary image representing cell boundaries was obtained by repeated use of filters and image operations and was used to construct a polygonal cellular lattice whose geometric properties were calculated. Four-cell vertices were manually tracked in 6–10 embryos for each genotype. To identify cells involved in rosette formation, all cells in a 40× field at the onset of intercalation in stage 7 were tracked for 20–25 min. To analyze interface dynamics, AP interfaces that were 3–7 μm long and oriented at 72°–108° relative to the AP axis (20% of the angular range) were measured in ImageJ at 1 min intervals starting 3–4 min before the increase in topological variance at stage 7.

Supplemental Data

Supplemental Data include color-coded pixel-intensity plots for Figures 1 and 3, images of cell patterns in fixed embryos, and time-lapse movies of wild-type and mutant embryos. These files are available at <http://www.developmentalcell.com/cgi/content/full/11/4/459/DC1/>.

Acknowledgments

We are grateful to Richard Zallen (Department of Physics, Virginia Tech) for many valuable discussions and for advice on the statistical analysis of cell patterns. We thank Keith Amonlirdviman for generously sharing an algorithm that we used as the basis for developing our computer program and Chris Field for providing Myosin II antibodies. We also thank Kathryn Anderson, Mary Baylies, Natalie Deneff, Mimi Shirasu-Hiza, Eric Wieschaus, and anonymous reviewers for comments on the manuscript. This work was supported by a Burroughs Wellcome Fund Career Award in the Biomedical Sciences, a March of Dimes Basil O'Connor Starter Scholar Research Award, and a Searle Scholar Award to J.A.Z.

Received: June 13, 2006

Revised: August 9, 2006

Accepted: September 12, 2006

Published: October 2, 2006

References

- Abdelilah-Seyfried, S., Cox, D.N., and Jan, Y.N. (2003). Bazooka is a permissive factor for the invasive behavior of discs large tumor cells in *Drosophila* ovarian follicular epithelia. *Development* 130, 1927–1935.
- Baum, B. (2004). Animal development: crowd control. *Curr. Biol.* 14, R716–R718.
- Benton, R., and St Johnston, D. (2003). A conserved oligomerization domain in *Drosophila* Bazooka/PAR-3 is important for apical localization and epithelial polarity. *Curr. Biol.* 13, 1330–1334.
- Bertet, C., Sulak, L., and Lecuit, T. (2004). Myosin-dependent junction remodelling controls planar cell intercalation and axis elongation. *Nature* 429, 667–671.
- Campos-Ortega, J.A., and Hartenstein, V. (1985). *The Embryonic Development of Drosophila melanogaster* (Berlin: Springer-Verlag).
- Chen, X., and Macara, I.G. (2005). Par-3 controls tight junction assembly through the Rac exchange factor Tiam1. *Nat. Cell Biol.* 7, 262–269.
- Chou, T.B., and Perrimon, N. (1992). Use of a yeast site-specific recombinase to produce female germline chimeras in *Drosophila*. *Genetics* 131, 643–653.
- Classen, A.-K., Anderson, K.I., Marois, E., and Eaton, S. (2005). Hexagonal packing of *Drosophila* wing epithelial cells by the planar cell polarity pathway. *Dev. Cell* 9, 805–817.
- Concha, M.L., and Adams, R.J. (1998). Oriented cell divisions and cellular morphogenesis in the zebrafish gastrula and neurula: a time-lapse analysis. *Development* 125, 983–994.
- Elul, T., and Keller, R. (2000). Monopolar protrusive activity: a new morphogenic cell behavior in the neural plate dependent on vertical interactions with the mesoderm in *Xenopus*. *Dev. Biol.* 224, 3–19.

- Foe, V.E., Field, C.M., and Odell, G.M. (2000). Microtubules and mitotic cycle phase modulate spatiotemporal distributions of F-actin and myosin II in *Drosophila* syncytial blastoderm embryos. *Development* 127, 1767–1787.
- Franke, J.D., Montague, R.A., and Kiehart, D.P. (2005). Nonmuscle Myosin II generates forces that transmit tension and drive contraction in multiple tissues during dorsal closure. *Curr. Biol.* 15, 2208–2221.
- Fristrom, D. (1988). The cellular basis of epithelial morphogenesis. A review. *Tissue Cell* 20, 645–690.
- Hardin, J. (1989). Local shifts in position and polarized motility drive cell rearrangement during sea urchin gastrulation. *Dev. Biol.* 136, 430–445.
- Harris, T.J., and Peifer, M. (2004). Adherens junction-dependent and -independent steps in the establishment of epithelial cell polarity in *Drosophila*. *J. Cell Biol.* 167, 135–147.
- Harris, T.J., and Peifer, M. (2005). The positioning and segregation of apical cues during epithelial polarity establishment in *Drosophila*. *J. Cell Biol.* 170, 813–823.
- Hartenstein, V., and Campos-Ortega, J.A. (1985). The spatio-temporal pattern of embryonic cell divisions. *Roux's Arch. Dev. Biol.* 194, 181–195.
- Hutterer, A., Betschinger, J., Petronczki, M., and Knoblich, J.A. (2004). Sequential roles of Cdc42, Par-6, aPKC, and Lgl in the establishment of epithelial polarity during *Drosophila* embryogenesis. *Dev. Cell* 6, 845–854.
- Hyodo-Miura, J., Yamamoto, T.S., Hyodo, A.C., Iemura, S., Kusakabe, M., Nishida, E., Natsume, T., and Ueno, N. (2006). XGAP, an ArfGAP, is required for polarized localization of PAR proteins and cell polarity in *Xenopus* gastrulation. *Dev. Cell* 11, 69–79.
- Irvine, K.D., and Wieschaus, E. (1994). Cell intercalation during *Drosophila* germband extension and its regulation by pair-rule segmentation genes. *Development* 120, 827–841.
- Jacinto, A., Wood, W., Woolner, S., Hiley, C., Turner, L., Wilson, C., Martinez-Arias, A., and Martin, P. (2002). Dynamic analysis of actin cable function during *Drosophila* dorsal closure. *Curr. Biol.* 12, 1245–1250.
- Keller, R., Davidson, L., Edlund, A., Elul, T., Ezin, M., Shook, D., and Skoglund, P. (2000). Mechanisms of convergence and extension by cell intercalation. *Philos. Trans. R. Soc. Lond. B Biol. Sci.* 355, 897–922.
- Kiehart, D.P., Galbraith, C.G., Edwards, K.A., Rickoll, W.L., and Montague, R.A. (2000). Multiple forces contribute to cell sheet morphogenesis for dorsal closure in *Drosophila*. *J. Cell Biol.* 149, 471–490.
- Kobieliak, A., Pasolli, H.A., and Fuchs, E. (2004). Mammalian formin-1 participates in adherens junctions and polymerization of linear actin cables. *Nat. Cell Biol.* 6, 21–30.
- Kovacs, E.M., Goodwin, M., Ali, R.G., Paterson, A.D., and Yap, A.S. (2002). Cadherin-directed actin assembly: E-cadherin physically associates with the Arp2/3 complex to direct actin assembly in nascent adhesive contacts. *Curr. Biol.* 12, 379–382.
- Lecaudey, V., and Gilmour, D. (2006). Organizing moving groups during morphogenesis. *Curr. Opin. Cell Biol.* 18, 102–107.
- Martin, P., and Lewis, J. (1992). Actin cables and epidermal movement in embryonic wound healing. *Nature* 360, 179–183.
- Muller, H.A., and Wieschaus, E. (1996). *armadillo*, *bazooka*, and *Stardust* are critical for early stages in formation of the zonula adherens and maintenance of the polarized blastoderm epithelium in *Drosophila*. *J. Cell Biol.* 134, 149–163.
- Munro, E.M., and Odell, G.M. (2002). Polarized basolateral cell motility underlies invagination and convergent extension of the ascidian notochord. *Development* 129, 13–24.
- Nance, J. (2005). PAR proteins and the establishment of polarity during *C. elegans* development. *Bioessays* 27, 126–135.
- Nikolaidou, K.K., and Barrett, K. (2005). Getting to know your neighbours; a new mechanism for cell intercalation. *Trends Genet.* 21, 70–73.
- Ninomiya, H., Elinson, R.P., and Winklbauer, R. (2004). Anteroposterior tissue polarity links mesoderm convergent extension to axial patterning. *Nature* 430, 364–367.
- Nusslein-Volhard, C., Frohhofer, H.G., and Lehmann, R. (1987). Determination of anteroposterior polarity in *Drosophila*. *Science* 238, 1675–1681.
- Oda, H., and Tsukita, S. (2001). Real-time imaging of cell-cell adherens junctions reveals that *Drosophila* mesoderm invagination begins with two phases of apical constriction of cells. *J. Cell Sci.* 114, 493–501.
- Oda, H., Uemura, T., Harada, Y., Iwai, Y., and Takeichi, M. (1994). A *Drosophila* homolog of cadherin associated with armadillo and essential for embryonic cell-cell adhesion. *Dev. Biol.* 165, 716–726.
- Petronczki, M., and Knoblich, J.A. (2001). DmPAR-6 directs epithelial polarity and asymmetric cell division of neuroblasts in *Drosophila*. *Nat. Cell Biol.* 3, 43–49.
- Redd, M.J., Cooper, L., Wood, W., Stramer, B., and Martin, P. (2004). Wound healing and inflammation: embryos reveal the way to perfect repair. *Philos. Trans. R. Soc. Lond. B Biol. Sci.* 359, 777–784.
- Riggleman, B., Schedl, P., and Wieschaus, E. (1990). Spatial expression of the *Drosophila* segment polarity gene *armadillo* is post-transcriptionally regulated by wingless. *Cell* 63, 549–560.
- Royou, A., Field, C., Sisson, J.C., Sullivan, W., and Karsenti, R. (2004). Reassessing the role and dynamics of nonmuscle Myosin II during furrow formation in early *Drosophila* Embryos. *Mol. Biol. Cell* 15, 838–850.
- Schock, F., and Perrimon, N. (2002). Molecular mechanisms of epithelial morphogenesis. *Annu. Rev. Cell Dev. Biol.* 18, 463–493.
- Shih, J., and Keller, R. (1992). Cell motility driving mediolateral intercalation in explants of *Xenopus laevis*. *Development* 116, 901–914.
- Solnica-Krezel, L. (2005). Conserved patterns of cell movements during vertebrate gastrulation. *Curr. Biol.* 15, R213–R228.
- Tepass, U., and Hartenstein, V. (1994). The development of cellular junctions in the *Drosophila* embryo. *Dev. Biol.* 161, 563–596.
- Topczewski, J., Sepich, D.S., Myers, D.C., Walker, C., Amores, A., Lele, Z., Hammerschmidt, M., Postlethwait, J., and Solnica-Krezel, L. (2001). The zebrafish glypican knypek controls cell polarity during gastrulation movements of convergent extension. *Dev. Cell* 1, 251–264.
- Verma, S., Shewan, A.M., Scott, J.A., Helwan, F.M., den Elzen, N.R., Miki, H., Takenawa, T., and Yap, A.S. (2004). Arp2/3 activity is necessary for efficient formation of E-cadherin adhesive contacts. *J. Biol. Chem.* 279, 34062–34070.
- Wallingford, J.B., Fraser, S.E., and Harland, R.M. (2002). Convergent extension: the molecular control of polarized cell movement during embryonic development. *Dev. Cell* 2, 695–706.
- Weaire, D., and Rivier, N. (1984). Soap, cells, and statistics—random patterns in two dimensions. *Contemp. Phys.* 25, 59–99.
- Wei, S.Y., Escudero, L.M., Yu, F., Chang, L.H., Chen, L.Y., Ho, Y.H., Lin, C.M., Chou, C.S., Chia, W., Modolell, J., and Hsu, J.C. (2005). Echinoid is a component of adherens junctions that cooperates with DE-Cadherin to mediate cell adhesion. *Dev. Cell* 8, 493–504.
- Wieschaus, E., Sweeton, D., and Costa, M. (1991). Convergence and extension during germband elongation in *Drosophila* embryos. In *Gastrulation*, R. Keller, ed. (New York: Plenum Press), pp. 213–223.
- Wodarz, A., Ramrath, A., Kuchinke, U., and Knust, E. (1999). Bazooka provides an apical cue for Inscutable localization in *Drosophila* neuroblasts. *Nature* 402, 544–547.
- Wodarz, A., Ramrath, A., Grimm, A., and Knust, E. (2000). *Drosophila* atypical protein kinase C associates with Bazooka and controls polarity of epithelia and neuroblasts. *J. Cell Biol.* 150, 1361–1374.
- Wood, W., Jacinto, A., Grose, R., Woolner, S., Gale, J., Wilson, C., and Martin, P. (2002). Wound healing recapitulates morphogenesis in *Drosophila* embryos. *Nat. Cell Biol.* 4, 907–912.
- Young, P.E., Richman, A.M., Ketchum, A.S., and Kiehart, D.P. (1993). Morphogenesis in *Drosophila* requires nonmuscle myosin heavy chain function. *Genes Dev.* 7, 29–41.
- Zallen, J.A., and Wieschaus, E. (2004). Patterned gene expression directs bipolar planar polarity in *Drosophila*. *Dev. Cell* 6, 343–355.
- Zallen, J.A., and Zallen, R. (2004). Cell-pattern disordering during convergent extension in *Drosophila*. *J. Phys.: Condensed Matter* 16, S5073–S5080.